Light Metals 2012 *Edited by: Carlos E. Suarez*
TMS (The Minerals, Metals & Materials Society), 2012

MECHANISM OF TRANSPORT BETWEEN THE ANODE-BATH INTERFACE AND THE ACTIVE BUBBLE GENERATION SITES IN HALL-HÉROULT CELLS

[1]Sándor Poncsák, László I Kiss
[1]Université du Québec à Chicoutimi, 555, Blvd de l'Univeristé, Chicoutimi, QC, Canada, G7H 2B1

Electrolysis, transport mechanism, bubble, diffusion, convection, anode, adsorption

Abstract

During the last decades, many efforts were spent to investigate different aspects of the Hall-Héroult process in order to improve its design and operation. However, many questions remain unanswered due to the complexity of the process and the hostile environment. One of the still unclarified questions is the mechanism of the transport of CO/CO_2 gas between the active electrolysis sites and the bubble-evolving anode pores. Generally, during electrolysis in aqueous systems, the generated gas is dissolved and transported through the electrolyte, especially when the anode is impermeable. However, the solubility of CO_2 in the molten cryolite is poor and the anodes, used in aluminum industry, are highly porous. In this paper, different mechanisms of the CO/CO2 transport between the gas generating anode – bath interface and the bubble releasing sites are examined. The majority of the anode gas seems to be transported through a thin superficial layer of the porous anodes, while transport via the molten bath and gas adsorption by the anodes plays a secondary role

Introduction

In the aluminum electrolysis cell, carbon-oxide gas is produced by a multi-step electrochemical reaction at the anode. The oxygen, discharged from the oxygen-containing complex ions, is combined with the carbon of the anode. Even if CO is the thermodynamically favoured product at the high temperature of the Hall-Héroult cells, the electrochemical reaction releases mainly CO_2 due to the very high current density [1-4]. The CO is produced rather during the re-oxidation of the aluminum by the CO_2 and the reaction between CO_2 and the anodic carbon particles, floating in the bath [1,2,4].

The anode reaction takes place at the anode bottom surface in contact with the bath, especially at the pitch-binder matrix, which is consumed faster than the coke grains [5]. On the other hand, bubbles are generated after heterogeneous nucleation in certain superficial pores of the anode bottom (bubble generation sites). In fact, entrapped air or the residues of preceding bubbles in the pores can increase initial radii of curvature of the bubbles and thus reduce energy (overpressure) demand for nucleation.

Rayleigh developed an equation to give a general description of the dynamics during volume change of spherical bubbles surrounded completely by liquid [6].

$$R\ddot{R}+\frac{3}{2}\dot{R}^2=\frac{\Delta p}{\rho_L}-\frac{2\sigma}{\rho_L R}-\frac{4\eta\dot{R}}{\rho_L R} \qquad (1)$$

where R is the bubble radius, $\dot{R}$ and $\ddot{R}$ are the first and second derivates of radius by time, Δp is the overpressure of the gas, ρ_L is the liquid density and σ is the surface tension. The left side represents the acceleration of the gas-liquid interface. The right side is composed by the overpressure term (which is the force, driving the growth of a bubble), as well as the surface tension and the viscosity terms. The last two terms act against the bubble growth.

The Rayleigh's equation can be used to describe bubble dynamics in cavitation (bubble collapse), boiling, electrolysis, etc. Its general form can describe bubble growth in Hall-Héroult cells as well, by the appropriate choice of initial and boundary conditions. However, one must keep in mind, that when the equation of Raiyleigh is used, the impact of the solid-gas interface is completely neglected.

As the bubble grows, the surface tension term looses its importance and the bubble shape is determined mainly by the contact angle, inertia and buoyancy forces. The contact angle of the CO_2 bubble-molten cryolite-carbon anode system promotes a hemi-spherical shape while the buoyancy force flattens the bubble. However, before the detachment, the bubble is not big enough [7] to be considerably flattened. What is more, the use of a simplified spherical shape is enough to analyse the possible transport mechanisms of the CO_2 gas between the anode-bath interface and the bubble generation sites. This basic mechanism is still not clarified in the published literature. Theoretically, three options are possible:

- transport by diffusion and convection through the electrolytic bath;
- transport by diffusion through a thin superficial layer inside the highly porous anode;
- adsorption / desorption of the anodic gas on the anode surface.

The above three hypotheses were investigated. This paper presents the conclusions of this theoretical study. This question has mainly a theoretical interest as in industrial cells, the growth of the bubbles seems to be controlled mainly by coalescence [8]

Mathematical modeling

In the case of bubbles released by the anode, the following simplifications can be applied, independently of the mass transport mechanism:

- the liquid is incompressible;
- the CO_2 at 960 °C behaves as a perfect gas;
- the physical properties of the gas and the liquid are constants;
- the temperature, pressure and concentration distribution inside the bubble is homogenous;
- the initial growth rate is equal to zero ($\dot{R}_{(t=0)}=0$), while the initial acceleration is not ($R_{(t=0)}>0$) [12,13].

In all cases, 5 μm of radius, representing a typical anode pore dimension [9, 10], was chosen as the initial size of the bubble. This value by the term of $2\sigma / R_0$ determines the minimal overpressure necessary to avoid bubble collapse due to the curvature of the gas-liquid interface. The excess pressure of gas, permitting the bubble to grow at any moment can be written the following way:

$$\Delta p = p_{bubble} - \left(p^0 + \rho_L \cdot g \cdot h + \frac{2\sigma}{R} \right) \quad (2)$$

where p_{bubble} is the pressure inside the bubble, p^0 is the atmospheric pressure, g is the gravitational acceleration, h is the height of the liquid column above the bubble. The detachment size of 3-6mm was chosen in accordance to the observations of Utigard et al. [7]. A bubble generated in a Hall-Héroult cell is supposed to reach this size after 0.5-0.6 sec [8,11,12]. The bubble detachment frequency is determined by the Fourier analysis of the voltammogramme measured in the electrolysis cells, where the detachment frequency is not masked by the coalescence. All the models presented below were tested whether they are able to reproduce bubbles with the typical detachment size and frequency.

Transport of the anodic gas through the molten cryolite

Most applications producing gas bubbles by electrolysis are using aqueous solution of salts. In such systems, the gas is generally transported by the liquid from the wetted anode surface to the bubbles, especially when non-porous anodes are involved. In that case, the bubble growth is governed by the mass diffusion through a thin layer around the bubble in a stagnant liquid, for which the formula of Scriven [13] can be used:

$$R(t) = 2\beta \cdot \sqrt{D \cdot t} \quad (3)$$

where D is the gas diffusivity in the liquid, t is the time, β is a function of saturation and bulk concentrations as well as the liquid and gas densities [12]. This formula proposes that the bubble radius should be proportional to the square root of the time. Westerheide et al. [14] used with high-speed camera to film the formation of hydrogen bubbles by electrolysis in aqueous sulphuric acid – platinum electrode system, in order to determine the dependence of β on the above mentioned parameters. They found that hydrogen bubbles had small truncated sphere shape and in most cases, the growth rate of single bubbles followed the law proposed by Scriven. However, when at least two bubbles were formed at the cathode at the same time, the exponent of the time decreased from 0.5 to 0.23. This change is due to the impact of a second bubble on the first:

- competition can take place between neighbouring bubbles to collect the dissolved gas in the liquid;
- the turbulence, created by the detachment of a neighbouring bubble can transport fresh, saturated liquid toward the vicinity the first bubble;
- neighbouring bubbles can coalesce.

Westerheide et al [14] estimated a hydrogen concentration 8-24 times higher than that corresponding to the saturation. They observed as well the increase of bubble growth rate with current density and decreasing pH. However, bubbles formed by hydrogen are much smaller than the bubbles of any other gas (including CO_2), especially when formed under a solid surface.

The mass transport through the liquid can be controlled by diffusion or by convection. The electrolyte in industrial aluminum electrolysis cells is much more turbulent than the liquid in the experience of Westerheide et al. The fact that the bath is strongly agitated by the dynamic movement of the bubbles and by MHD effects makes the convection the dominant mechanism.

Gas transport controlled by diffusion through a stagnant liquid around the bubble

The saturation concentration and the diffusivity of CO_2 in molten cryolite are very low, only 3-5 mol m^{-3} and 10^{-5} – 10^{-8} cm^2/s respectively [15] at the temperature of electrolysis. Consequently the bath becomes oversaturated very fast in the vicinity of the anode and the gas concentration gradient can be very high between the bubble surface and the bulk.

In such case, the overpressure Δp in the Rayleigh equation (1) can be estimated for a perfect gas as shown below:

$$\Delta p = \frac{R_g \cdot T}{4\dot{R}} \cdot \sqrt{\frac{D}{\pi \cdot t}} \cdot \left(C_{b,l} - C_{\infty,l} \right) \quad (4)$$

where R_g is the universal gas constant, T is the absolute temperature and $C_{b,l}$, $C_{\infty,l}$ are the gas concentrations in the liquid (mol/m^3) at the bubble surface and in the bulk respectively. Equation 4 is written in spherical coordinates. Both the dry contact surface between the bubble and the anode and the deformation of the bubble by the buoyancy force are neglected. The first overestimates, while the second underestimates the transport surface area between the bubble and the bath. However, this computation is used only to estimate if the bubble can be blown up by diffusion. $C_{b,l}$ was considered being equal to the saturation concentration, while $C_{\infty,l}$ was computed by the equation of Bagotsky [16] with the assumption that it should correspond to the pressure necessary to nucleate a new bubble.

Gas transport controlled by convection in stirred liquid around the bubble

The detachments of the bubbles, their gliding under the anode and the coalescences between them provoke intensive mixing in the bath. In such case the mass transfer of the gas toward the bubble is controlled by convection:

$$\Delta p = \frac{R_g \cdot T}{4\dot{R}} \cdot h_g \cdot \left(C_{b,l} - C_{\infty,l} \right) \quad (5)$$

where h_g is the gas transfer coefficient between the bubble and liquid. The value of h_g (m/s) was estimated with the dimensionless empirical equation of liquid flow around a spherical shaped solid [17]. The fact that the bubble is relatively small before detachment and thus less deformable permits to use this assumption:

$$Sh = \frac{h_g \cdot R}{D} = 2 \quad \text{if Re} < 1$$

$$Sh = \frac{h_g \cdot R}{D} = \left(0.97 + 0.68 \cdot \mathrm{Re}^{0.5}\right) \cdot Sc^{0.3}$$
$$\text{if } 1 \le \mathrm{Re} < 2000 \qquad (6)$$

Due to the small size of the bubble and the observed velocities in the electrolysis cell, the Reynolds number can not be higher than 2000. Both the diffusion and the convection models were numerically evaluated with Maple.

Transport of the anodic gas through a thin layer inside the porous anode, close to the bottom

The prebaked carbon anodes, used in the Hall-Héroult process, contain 15-25% of interconnected pores [18,19]. Consequently, the anode is able to stock and transport the gas toward the growing bubbles. What is more, the penetration of this gas into the pores is promoted by the high gas pressure present due to the high generation rate and the low solubility of the CO_2 in the molten cryolite [20]. It was also observed that the electrolyte can not penetrate into the anode pores during electrolysis [21]. Ziegler [9] examined the main reason for the higher porosity at the prebaked anode bottom, compared to the rest of the anode. He found that the oxidation of the carbon by the CO_2 present in the pores can be the main factor. For all of those reasons, the diffusion of the gas through a thin layer of the anode bottom was examined. The diffusion of the CO_2 inside the anode can be described by the Fick's second law:

$$\frac{\partial C}{\partial t} = D_{CO_2,C} \nabla^2 C \qquad (7)$$

Where C and $D_{CO_2,C}$ are the concentration in $mol \cdot m^{-3}$ and the diffusivity of the CO_2 in the anode respectively. As the solubility of the CO_2 in the molten cryolite is low, the mass transfer toward the liquid can be neglected compared to the transport into the growing bubble through the dry contact spot between the anode and the bubble. In this case, the massetransfer toward the bubble can be written as shown below:

$$-D_{CO_2,C} \frac{\partial C}{\partial x} = h_g \cdot \left(C_a - C_b\right) \qquad (8)$$

This mechanism creates a fluctuation of the gas pressure in the pores of a thin layer at the anode bottom. Namely, the pressure increases when the surface in contact with the bath produces the gas by electrolysis at a high rate, and decreases when the growing bubble covers the surface and aspiring the gas stored in the pores.

Golovina [22] measured the variation of the diffusion coefficient of the CO_2 in porous carbon blocks ($D_{CO_2,C}$) with the temperature. She fitted a curve on her experimental results and obtained the following expression:

$$-D_{CO_2,C} = 2.2 \cdot 10^{-3} \left(\frac{T}{293.15}\right)^{1.34} \qquad (9)$$

This equation gives a value of $1.5 \cdot 10^{-2} cm^2/s$ at 960 °C, 3-6 orders of magnitude higher than the diffusion coefficient of the CO_2 in the electrolyte. Some permeability values can also be found in the literature, but they are quite different when compared to each others. In order to validate the results of Golovina, a diffusion model was built, based on the D'Arcy equation of fluid flow through a porous media. The similitude is based on the fact that the gas in the anode can only flow through the interconnected pores. The number of parallel channels (n) was replaced by the anode porosity (ε) and the real shape of the interconnected anode pores was considered by the tortuosity factor (ξ):

$$n = \frac{4\varepsilon \cdot V_T}{d^2 \cdot \pi \cdot l_{eff}} \qquad l_{eff} = l \cdot \xi \qquad (10)$$

where d, l and l_{eff} are the diameter, the length and the effective length of the channels respectively , while V_T is the total volume of the anode bloc studied. After insertion of equation 10 into well known equation of D'Arcy, the following formula was obtained:

$$\dot{V}_{gas} = \frac{1}{32} \cdot \frac{\varepsilon \cdot V_T \cdot d^2 \cdot \Delta p}{\eta \cdot \xi^2 \cdot l_{eff}^{\ 2}} \qquad (11)$$

Table 1 resumes the limit values used for the parametric analysis. As the value of the diffusivity coefficient given by Golovina lies between the extreme values obtained by this study, it was accepted for the diffusion model.

Table 1 Limit values used for the parametric analysis for diffusivity of CO_2 in the porous anode

Parameter	Lower limit	Upper limit
Irregularity factor*	1	10
Porosity	0.15	0.25
Average channel diameter [m]	$3 \cdot 10^{-6}$	$3 \cdot 10^{-4}$
Dynamic viscosity of the gas as the function of temperature [Pa·s]	$4.358 \cdot 10^{-5}$ (T=850 °C)	$4.778 \cdot 10^{-5}$ (T=1008 °C)

* the estimated tortuosity for carbon anode is 4.5-6.8 [23]

The gas diffusion in the anode, in the vicinity of a growing bubble was modeled with the finite element method, using COSMOS©. An elementary volume around the nucleation site, called influenced zone, was selected for this study. The elementary volume is cylindrical due to the axial symmetry of the bubble and the gas generation site is located at the center of the bottom of this volume (figure 1).

The axial symmetry permits to use only a segment of the cylinder in order to decrease the number of the nodes to 10 000 and thus accelerate the computation without loosing precision. By preliminary computations, the height of the cylinder was chosen 0.17 m, as at the distance from the anode bottom no significant fluctuations of the concentration can be observed.

The model used the following assumptions:

- The current remains constant in the Hall-Héroult cell; consequently it is independent of the bubble covering, which modifies only the local current density;

- There is no accumulation or depletion of gas over the bubble generation cycles; consequently all the gas generated during one cycle is evacuated by the given bubble;
- There is no mass exchange between neighbouring finite elements, consequently the perimeter of the cylindrical elementary volume is isolated;
- The elementary volumes of the anode bottom participate in the gas generation or in the gas transport, depending on the fact if they are covered by the electrolyte or the bubble.

A macro was written to compute bubble volume and equivalent spherical radii at every time step, using the Rayleigh equation. Then, the shape and the characteristic dimensions (contact radius, maximal horizontal radius, height) of the growing bubble were computed, using the equilibrium shape of a sessile bubble in CO_2-carbon-molten cryolite system [24].

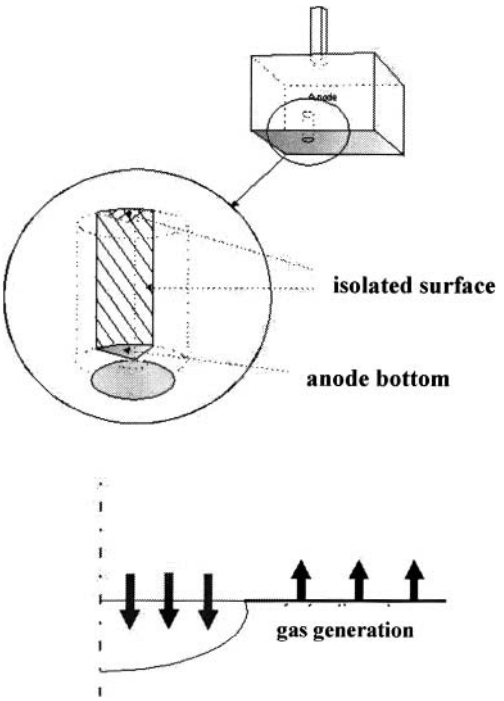

Figure 1 – Computational domain for the study of the gas transport through the anode pores

The internal duct flow correlations cannot be used here to estimate the mass transfer coefficient due to the different size of the gas-solid interfaces and the direction of the fluid flow compared to the orientation of the anode bottom. For this reason, the transport coefficient of the gas between the solid and the bubble was used as a variable.

Transport of the anodic gas by adsorption and desorption on the anode surface

Due to the already mentioned low solubility of CO_2 in the molten cryolite and the high gas production rate, the electrolytic bath close to the anode bottom becomes quickly oversaturated. In that case, a part of the excess CO_2 can be adsorbed by the carbon based anode surface. This phenomenon can be important especially if a vitreous (non-porous) anode is involved. On the other hand, the CO_2 adsorbed on the internal surface of the pores must be transported through the pores by diffusion and thus must be treated by the anode diffusion model

In an adsorption-desorption (**AD**) model, a given area of the anode bottom produces CO_2 gas by electrolysis as long as it is in contact with the bath. As soon as a growing bubble reaches and covers the area in question, the electrolysis is blocked and the adsorbed CO_2 starts to be released by desorption and enters into the bubble, driving its growth.

Adsorption of CO_2 on carbon-based materials has been extensively studied during the last hundred years [cited in 25]. The practical importance of this phenomenon is related to the fact that the anode is consumed in CO_2 atmosphere by the Boudouard reaction. A consensus seems to be established that the Langmuir model can be used to describe CO_2 adsorption by carbon based materials, especially at relatively low pressure ranges [cited in 25-27]. Furthermore, the presence of multiple layers of adsorbed gas on the anode surface during aluminum electrolysis should block the anode reaction. This model assumes that all adsorbing sites are energetically equivalents and can hold only one adsorbed molecule (monolayer model). Any interaction among the adsorbed molecules is neglected. The details of the Langmuir model, used by the authors, are presented in several papers [25-27].

Results and discussion

The pure diffusion model used for stagnant liquid gives a very slow increase of equivalent bubble radius due to the very low diffusivity of CO_2 in the molten cryolite (figure 2). As the initial growth rate of the bubble was not known, a parametrical study by varying the diffusion coefficient was carried out. Figure 2 shows that even a big change of that parameter does not affect significantly the growth curve.

The convection model coupled with the equation of Raleigh gives a much faster bubble growth rate (figure 3). The curve seems to be nearly linear with the exception of the first second, where the surface tension plays an important role. However, even when the convection model is used, the bubble grows too slowly; the equivalent radius of 3 mm is reached only after 100 seconds.

The gas diffusion through the porous anode seems to give satisfying results, as the typical detachment size of the bubble reached after 0.2-0.3 seconds (figure 4). This is in accordance with the fact that the diffusivity of CO_2 in a porous anode is much higher than in the bath. d, d_c and h represent the maximal diameter (detachment diameter), the contact diameter and the height of the bubble respectively. d and d_c are close each other since the typical contact angle value in the molten cryolite-carbon-CO_2 system is close to 90°. On the other hand, as the bubble is growing, the surface tension looses its importance and the bubble becomes more and more flattered due to the buoyancy force. Consequently, the height increases much slower than the horizontal dimensions which is well shown in figure 4.

An example of the molar concentration distribution inside the anode, in the vicinity of the growing bubble is shown in figure 5. The gas concentration is high at the anode bottom in contact with the bath (where the CO_2 is generated), while the zone near the

bubble-solid interface is poor in gas. Figure 6 shows an example of the molar concentration distribution of gas inside the anode at difference distances from the anode bottom. The anode lower surface is approached in the figure when advancing from left to right. A significant special variation of gas concentration can only be observed in a thin layer of about 3mm, in the vicinity of the anode bottom (figure 4 and 7).

The pattern of the gas concentration distribution in the anode is similar during the whole period of an individual bubble growth; however, the concentration values are varying in time and depend on gas transfer coefficient value between the anode and the bubble. The concentration variation in time can be neglected over a distance of 1.3mm from the anode bottom (figure 7). The different curves show the variation of the gas concentration at central axis and at any point of the perimeter of an elementary bubble generating volume at different moments of a bubble growing cycle.

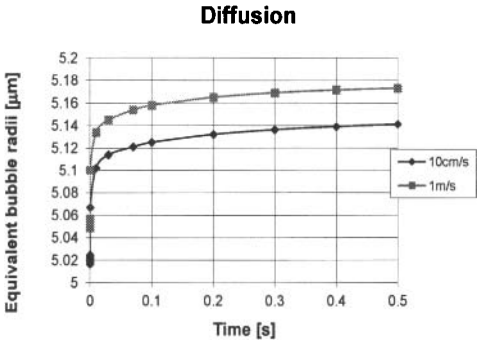

F

igure 2. Growth of the bubble, controlled by gas diffusion through the liquid, with different initial growing rate.

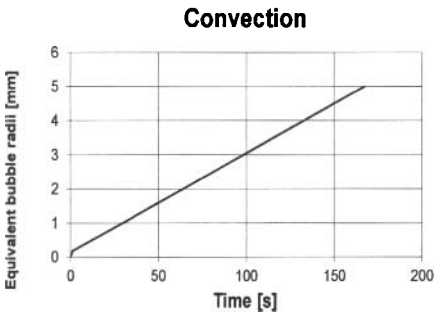

Figure 3. Growth of the bubble, controlled by convection of the gas in the liquid.

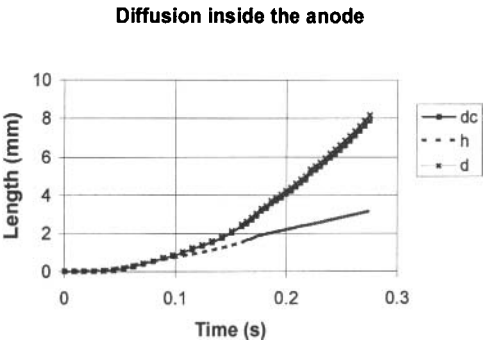

Figure 4. Variation of the characteristic dimensions of the growing bubble, computed with the gas diffusion in anode model.

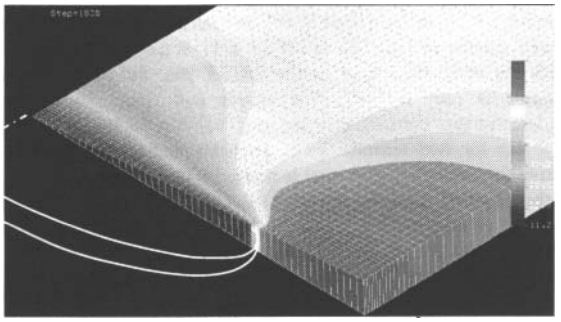

Figure 5. Example of the concentration (mol/m^3) distribution of the CO_2 inside of the anode, in the vicinity of a growing bubble at the anode bottom.

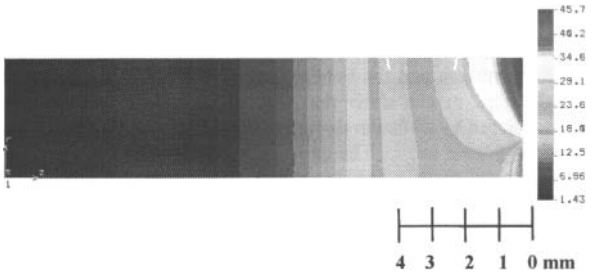

Figure 6. Example of the concentration (mol/m^3) distribution of the CO_2 in a plan vertical and perpendicular to the anode bottom

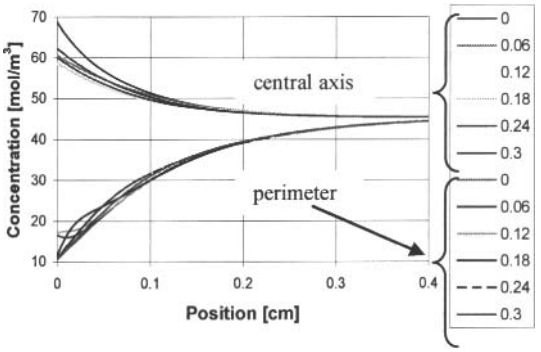

Figure 7. Evolution of the molar concentration of CO_2 at the center axis and at the perimeter of elementary gas generating volume at different moments of a bubble growth cycle

Diffusion

A half-spherical bubble with a radius of 3 mm contains $5.76 \cdot 10^{-7}$ mol CO_2 gas at 960 °C and 104.4 kPa (sum of the atmospheric and hydrostatic pressure of the bath). This amount of CO_2 can be produced by a $4.94 \cdot 10^{-5}$ m^2 circular anode surface around the bubble during 0.5 seconds, using a current density of 0.9 A/cm^2. That surface corresponds to a gas generating elementary surface for one bubble (***GGES***). If one supposes, that all the CO_2 is adsorbed by the internal surface of the pores of an elementary anode volume (***EAV***) in the vicinity of the nucleation site, before being transported toward a bubble, the minimally necessary storing volume can be computed the following simple way.
One CO_2 molecule can cover about $3.3 \cdot 10^{-10}$ x $7 \cdot 10^{-11}$ m^2. $5.76 \cdot 10^{-7}$ mol CO_2 distributed tightly covers at least $7.98 \cdot 10^{-3}$ m^2. Considering that the specific surface of the prebaked anode is around $1.5 \cdot 10^6$ m^2/m^3 [cited in 10], that surface can be found in an anode volume of $5.32 \cdot 10^{-9}$ m^3. If the ***EAV*** is a cylindrical volume, with the same base area as the ***GGES*** has, the height of that volume is only 0.1mm. This simple and rough computation underestimates considerably the real volume necessary to store that gas for two reasons. First, probably not all the surface is active for adsorption and what is more, an important portion of the carbon surface must be liberated as it participates in the anodic reaction. However, this computation proves that an important portion of the gas can be stored in adsorbed form.
Is it difficult to find in the literature precise desorption coefficient data for prebaked anodes. For this reason, the estimation of the contribution of adsorption-desorption to the gas transport needs further study.

Conclusion

Different gas transport mechanisms between the gas producing anode surface and the bubble generating sites were studied. The calculated results show that the major part of the gas can be transferred by diffusion through a thin layer (less than 3mm thick) of the porous anode. The gas transport by convection through the electrolyte plays a secondary role due to the low diffusivity of CO_2 in the molten cryolite and the presence of a thin laminar sub-layer around the bubbles even in a well stirred bath. Gas adsorption and desorption can play a role in gas storage. Its role can become dominant when non-porous anodes (such as vitreous graphite) are used. The different gas transport mechanisms influence the dynamics of the growth of individual bubbles in their early life, while they are relatively small. However, other research shows that the coalescence remains the determining growth mechanism for macro-bubbles.

References

1. E.W. Dewing, *The chemistry of the alumina reduction cell*, Canadian Metal. Quarterly, 30 (3) (1982), 153-161
2. A.T Tabereaux, N.E. Richards and C.E. Satchel, *Composition of reduction cell anode gas during normal conditions and anode effect*, TMS Light Metals, (1995) , 325-333
3. R.F. Wharton and B.J. Welch, *Chemical and electrochemical oxidation of heterogeneous carbon anodes*, Electrochimica Acta, 25 (1980), 217-221
4. J. Thonstad, *On the anode gas reaction in aluminum electrolysis II*, Journal of the Electrochem. Soc., 111 (8) (1964), 959-965
5. J. Thonstad, *Reaction mechanism and wear of anodes in aluminium electrolysis*, VI. Aluminium Symposium, (1973), 75-86
6. L. Rayleigh, Phil. Mag. 34. 94. (1917)
7. T. Utigard, J.M. Toguri and S.W. Ip, *Direct observation of the anodic effect by radiography*, TMS Light Metals, (1988), 703-706
8. L. Kiss and S. Poncsák, *Effect of the bubble growth mechanism on the spectrum of voltage fluctuations in the reduction cell*, TMS Light Metals (2002), 217-223
9. L.P. Lossius et al., *Mass loss, fume and porosity studies of pitch + dust binder matrix for anodes*, Ligth Metals, (1996), 515-520
10. D.P. Ziegler, *Sub-surface carbon dioxide reaction in anodes*, TMS Light Metals, (2011), 901-906
11. N. Richards and al., *Characterization of the fluctuation in anode current density and "bubble events" in industrial reduction cells*, TMS Light Metals, (1993), 315-322
12. K. E. Einarsrud and E Sandnes, *Anodic voltage oscillations in Hall-héroult Cells*, TMS Light Metals, (2011), 555-560
13. L.E. Scriven, *On the dynamics of phase growth*, Chem. Eng. Sci., 10 (1959), 1-13
14. E. Westerheide and J. Westwater, *Isothermal growth of hydrogen bubble during electrolysis*,Am. Inst. of Chem. Eng. AICHE Journal, 7 (3) (1961), 357-362
15. M. Rolin, *L'électrolyse de l'aluminium*, Inst. Nat. des Sci. Appl. de Lyon (1981) (p2-14)
16. V.S. Bagotzky, *Fundamentals of electrochemistry*, Translated from Russian by Klaus Muller, Plenum Press, New York (1992) (p2-72)
17. F. Kreith, *Principles of heat transfer*, 2nd edition, Int. Textbook Co. Scrancton, Pennsylvania (1965) (2-77)
18. R&D Carbon Ltd, *Anodes for aluminum industry*, 1st edition, Sierre, Switzerland, (1995)
19. H. Marsh, *Introduction to carbon science*, Proc. Of Short Cours, Univ. of Newcastle, England, 12-16th September 1988
20. S. Wilkening, *Reflection on the carbon consumption of prebaked anodes*, Light Metals, (1995), 715-724
21. J Horvath, *Plant Measurements at Hungalu aluminium Smelters*, Internal Report, Hungalu R&D Center Aluterv FKI, Hungary, (1984)
22. E.C. Golovina, *The question of the gas diffusion in the carbon*, Doklady Akademii Nauk, Russia 1 (1952), 141-144
23. P.L. Walker and F. Rusinko, *Gasification of carbon rods with carbon dioxide*, J. Phys. Chem., 59 (1955), 241
24. S. Hartland and R. Hantley, Axisymmetric fluid-liquid interfaces, Tables giving the shape of sessile and pending drops and external menisci, with example of their use, Elsevier Sci. Pub. Group, Amsterdam (1976)
25. C.M. White et al., *Sequestration of carbon dioxide in coal with enhanced coalbed methane recovery – A Review*, Energy and Fuels, 19 (3) (2005), 659-724
26. Shabi Ulzama, A theoretical analysis of single coal particle behaviour during spontaneous devolatilization and combustion, Dissertation Dr. Ing., Otto-von-Guericke-Universitat, Magdeburg, April 2, 2007
27. X.Jian, P. Guan and W. Zhang, *Carbon dioxide sorption and diffusion in coals: experimental investigation and modeling*, Sci. China; Earth Sci. DOI 10.1007/s11430-011-4272-4